Collaborative Mobile Target Imaging in UWB Wireless Radar Sensor Networks

Muharrem Arik, *Student Member, IEEE* and Ozgur B. Akan, *Senior Member, IEEE*

***Abstract*—Wireless sensor networks (WSN) have thus far been used for detection and tracking of static and mobile targets for mission critical surveillance applications. However, detection and tracking do not suffice for a complete and accurate target classification. In fact, surveillance target imaging yields the most valuable information. Current techniques mainly aim to provide images of static environment in a sensor network. Nevertheless, imaging of mobile targets requires networked and collaborative detection, tracking and imaging capabilities. With this regard, ultra-wideband (UWB) radar technology stands as a promising approach for networked target imaging due to its unique features such as having no line-of-sight (LoS) requirement. However, UWB wireless radar sensor network (WRSN) is yet to be developed for imaging of mobile targets. In this paper, an architecture and a new collaborative mobile target imaging (CMTI) algorithm for WRSN are presented. The objective is to efficiently obtain an accurate image of mobile targets based on the collaborative effort of deployed radar sensor nodes. CMTI enables detection, tracking and imaging of mobile targets as a complete WRSN solution. Performance evaluations reveal that CMTI yields high quality radar image of mobile targets in WRSN with very low communication overhead regardless of the target shape and velocity.**

***Index Terms*—Mission Critical Networks, Wireless Radar Sensor Networks, Mobile Target Imaging, CMTI, Radar Imaging.**

I. Introduction

WIRELESS Radar Sensor Network (WRSN) is emerging as an enabling technology for applications such as border surveillance, intrusion monitoring for unauthorized movement of targets around critical facilities. Surveillance applications, i.e., real-time detection, tracking and classification of intrusion, require mission critical networking capabilities in wireless sensor networks (WSN).

Generally, low power ultra-wideband (UWB) radar sensors are used in detection, tracking and localization of an intruder in sensor field [4], [5], [6], [7], [12]. However, detection and tracking do not suffice for a complete target classification in mission critical surveillance applications. To address this need, target imaging is imperative to effectively determine the features of the mobile target.

Manuscript submitted 1 April 2009; revised 21 October 2009. This article was originally assigned to the June 2010 Mission Critical Networking issue of IEEE Journal on Selected Areas in Communications.

This work was supported in part by the Turkish Scientific and Technical Research Council (TUBITAK) Career Award under grant #104E043 and by the Turkish National Academy of Sciences Distinguished Young Scientist Award Program (TUBA-GEBIP).

The authors are with the Next-generation Wireless Communications Laboratory (NWCL), Department of Electrical & Electronics Engineering, Middle East Technical University, Ankara, Turkey (e-mail: {arik,akan}@eee.metu.edu.tr).

Digital Object Identifier 10.1109/JSAC.2010.100820.

Object detection and imaging via sensor network is presented in [4], with multi-static imaging of fixed objects or invariant environment by using mobile radar sensors. Here, to obtain high quality radar image, large number of samples of the object need to be taken and transported to the sink, which incur huge amount of traffic, and hence, potentially lead to congestion in the network. Furthermore, radar image quality and communication challenges are not investigated in [4].

In fact, UWB radar technology can be used for networked collaborative target imaging over a field due to its unique features. UWB radar sensors can provide detection, localization and imaging of targets in short range regardless of environmental conditions [4], as they can operate in all weather conditions, including fog, rain, sleet, hail, snow, and sand. In the classification process, UWB radar image of the mobile target is required to accurately assess the threat level of the mobile intruder. Spatially distributed radar sensor nodes can gather significant information, e.g., feature and shape, on mobile targets in sensor field. However, UWB-based WRSN is yet to be developed for high quality imaging of mobile targets.

In this paper, we introduce an architecture for UWB wireless radar sensor network and a new collaborative mobile target imaging (CMTI) algorithm. The algorithm seeks to accurately and efficiently obtain image of mobile targets based on the collaborative effort of deployed UWB radar sensor nodes. It uses static radar sensor nodes for tracking and imaging process and exploits movement of the target in sensor field to build its own multi-static radar synthetic aperture. Then, CMTI forms an image of the mobile target relative to the deployment of the radar sensor nodes, the target mobility and radar cross section (RCS) of the target. It incorporates the smallest range resolution selection with threshold (SRRS-th) component to improve quality of radar images. CMTI also adopts forward error correction (FEC) scheme to provide reliable transport of observations to sink over multi-hop paths. Importantly, the imaging part of CMTI mainly runs on the sink and CMTI does not require complex operations at resource-constrained radar sensor nodes. It yields high quality radar image in a communication efficient way using multi-static radar structure of radar sensors in WRSN.

The remainder of the paper is organized as follows. In Section II, the proposed WRSN structure is introduced and the architecture of the radar nodes are explained. In Section III, the collaborative mobile target imaging, CMTI, is presented in detail along with its all phases. Error analysis of CMTI is discussed in Section IV, where the sources of error affecting image quality are pointed out. In Section V, performance evaluation is presented and the results are discussed. Finally, concluding remarks are given in Section VI.

II. Wireless Radar Sensor Network Architecture

WRSN is built of two-layered structure, i.e., *target detection layer*, and *target imaging layer* as in Fig. 1. Target detection layer is composed of magnetic, ultrasonic or seismic sensors for motion detection process. These sensors are assumed to be always awake and have only mobile target detection feature. They communicate the area and time of detection to the sink. Target imaging layer has UWB radar sensors to be used for radar imaging of mobile targets. To minimize energy consumption, the target imaging layer is not always active. Once a target is detected, sink can wake up the radar sensor nodes in target imaging layer over the region of detection, i.e., *event field*.

WRSN is composed of short range low power radar sensor nodes with low hardware complexity and capability of specifying accurate radar range profile of mobile targets in a power-efficient way. In target imaging layer, there are two types of radar sensor nodes, i.e., *anchor* as an UWB radar transmitter and *observer* as an UWB receiver. Observer is equipped with UWB receiver, and can sense UWB signals coming from the environment. Anchor has a capability of generating coded impulses with UWB transmitter.

Observer employs a simple correlation receiver, which compares an interval of received signal with a reference signal and operates based on the principle of *range-gating*. Analog-to-digital (A/D) converter of the receiver samples only those return signals that fall in a narrow time window, i.e., *range-gate* [7]. Hence, some part of the observation can be taken during each transmitted pulse interval by sweeping range-gate with a delay. After a certain time, complete set of samples of the entire signal can be obtained. Here, it is assumed that returning pulses do not change during several pulses long. For range measurement, observer uses time difference of arrival (TDoA).

Note that clutter is one of the main problems for the radar receivers, as there exist many clutters in the environment due to large UWB receiver bandwidth. Here, only time-invariant clutters are assumed to exist, and a basic moving target filter is used to avoid static clutter effect in the observer architecture. A basic averaging background subtraction technique is used [15] for the simplicity of observer. The anchor node hardware consists of impulse generators which generate compressed impulses in a pseudo-random manner. Impulse generator generates Gaussian impulses with anchor pulse-width (PW).

Anchor radar transmitted power affects its power consumption and the network lifetime. To minimize power consumption, anchor minimum transmitted power, (P_{min}^{anc}), must be found, which provides accurate sensing of mobile target at maximum range. To this end, firstly, minimum required power for accurate sensing in the observer, P_{th}, needs to be calculated. To find P_{th}, signal-to-noise ratio (SNR) at the observer must be expressed. Each anchor-observer pair composes a bistatic radar structure. In a bistatic radar, with narrowband (NB) pulses, the received power, P_{obs}, can be evaluated by using the Friis' formula [5], which does not hold in UWB domain as the wavelength may vary within the signal's large band. Thus, the Friis' formula over all wavelengths should be integrated over the frequency interval

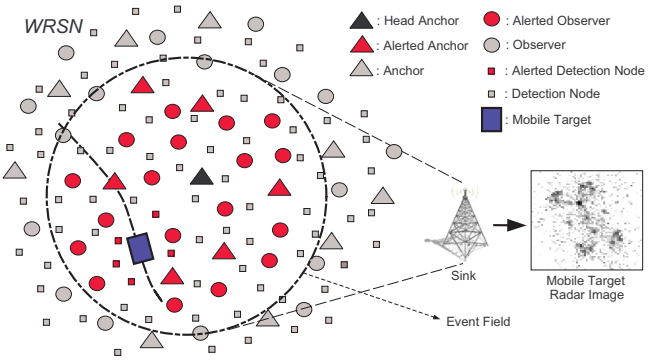

Fig. 1. Wireless Radar Sensor Network (WRSN) architecture.

$[f_L, f_U]$ [5], [16]. For the anchor-target-observer multi-path,

$$P_{obs}^{UWB} = \int_{f_L}^{f_L+B} \frac{S_{anc}(f)\, G_{anc}(f)\, G_{obs}(f)\, \sigma_B}{(4\pi)^3 \left(R_{anc}^2\, R_{obs}^2\right)} \left(c/f\right)^2 \mathrm{d}f \tag{1}$$

where $S_{anc}(f)$ is the one-sided transmitted power spectral density (PSD), $G_{anc}(f)$, $G_{obs}(f)$ are the frequency-dependent antenna gains, $B = f_U - f_L$ is bandwidth, c is the speed of light, σ_B is the object bistatic RCS, R_{anc} and R_{obs} are the distances from anchor and observer to object, respectively. Considering a white spectrum for the transmitted signal from anchors, constant antenna gains and constant RCS over frequencies $[f_L, f_U]$, then (1) becomes [5],

$$P_{obs}^{UWB} = \frac{S_{anc}\, G_{anc}\, G_{obs}\, \sigma_B\, c^2}{(4\pi)^3 \left(R_{anc}^2\, R_{obs}^2\right)} \left(\frac{1}{f_L} - \frac{1}{f_L + B}\right) \tag{2}$$

where S_{anc} is the transmitted PSD, G_{anc}, G_{obs} are the constant antenna gains. Then, SNR is,

$$SNR_{UWB} = \left[N_s\, P_{obs}^{UWB}\right] / \left[N_0\, PRF\right] \tag{3}$$

where P_{obs}^{UWB}/PRF is the received energy per scattered pulse, N_s is the processing gain, N_0 is the noise power at the observer and PRF is the pulse repetition frequency of the UWB transmitter at anchor. For typical correlation detection in the observer receiver, we assume that the threshold SNR at maximum range is SNR_{th}. Then, P_{th} is expressed as

$$P_{th} = \left(SNR_{th}\, N_0\, PRF\right) / N_s \tag{4}$$

As observed in (3), PRF used by the anchor needs to be minimized to improve the received signal quality at the observer or to minimize threshold power level in (4).

Observer nodes use equivalent-time sampling method in their UWB receivers. For gathering a complete signal, $S \times RG_w$ seconds is required at the receiver. S is the total number of samples for gathering a complete observation and RG_w is the range-gate width. The receiver requires, $T_\sigma = S/F_{ADC}$ seconds, where F_{ADC} is the observer A/D converter sampling frequency. Besides, PRF for anchor must be linearly dependent to F_{ADC} at the observer, i.e., $PRF = k\, F_{ADC}$, which yields $PRF = k\, S/T_\sigma$, where k is any positive integer. Here, we try to minimize PRF to minimize threshold received power P_{th} at the observer. For minimum PRF, k is selected as 1 and minimum PRF becomes S/T_σ. However, there is a limitation on PRF, while mobile target is sensing as in [8],

[9]. In mobile target scenario, a relation is detailed for devices which use equivalent-time sampling method in [8] as,

$$4\,T_\sigma\,V_{max} < (c/B) \tag{5}$$

where V_{max} is the maximum mobile target radial velocity to observer, B is bandwidth, c is the speed of light. This is due to the assumption that the target should move smaller than the half of the range resolution of the transmitted pulse in T_σ, then, we safely assume the time-invariance of the received signal [8]. This yields that the total received signal with equivalent-time sampling is almost the same as the real signal.

Hence, when k is 1, (5) becomes $(4\,S\,V_{max})/PRF < (c/B)$ and minimum value for PRF becomes, $PRF_{min} = (4\,V_{max}\,B\,S)/c$. Thus, PRF_{min} changes linearly with maximum mobile target radial velocity.

By using PRF_{min} for a selected V_{max}, received power threshold required for accurate detection is

$$P_{th} = (SNR_{th}\,N_0\,PRF_{min})\,/N_s \tag{6}$$

Then, when $P_{obs}^{UWB} \geq P_{th}$ and $P_{min}^{anc} = S_{min}^{anc}B$, minimum transmitted power can be found from (2) as

$$P_{min}^{anc} = \frac{P_{th}\,(R_{anc}\,R_{obs})_{max}^2\,(4\pi)^3}{G_{anc}\,G_{obs}\,\sigma_B\,[\frac{1}{f_L} - \frac{1}{f_L+B}]\,c^2}B \tag{7}$$

where, $(R_{anc}\,R_{obs})_{max}$ is the maximum value of the anchor and observer distance to the target and equal to $((R_{anc} + R_{obs})^2)/4$.

Each anchor transmits its compressed pulses with minimum power level P_{min}^{anc} for accurate sensing at maximum range. This power level can be adjusted based on the maximum sensible velocity V_{max} set by a specific mission critical network application. Increasing transmit power for increasing the maximum bistatic range adversely effects the main system performance parameter V_{max}. Users may select the maximum bistatic range in WRSN with considering V_{max}.

III. Collaborative Mobile Target Imaging (CMTI)

The objective of CMTI algorithm is to efficiently obtain an accurate image of mobile targets based on the collaborative effort of deployed UWB wireless radar sensor nodes. CMTI is adaptive to mobile target velocity and direction and can be configured according to the required level of image quality. CMTI is a five-phase algorithm. Its operation starts with *Initialization Phase* as explained in Section III-A. In this phase, sink selects anchors, called *Head Anchor* (HA), performs clustering, and initializes all detection sensors as in Fig. 1. If any detection occurs, it awakes radar nodes in the alerted cluster.

Target Tracking and *Inverse Synthetic Aperture Capturing (ISAC)* phases are operated over the entire field in the HA. *Target Tracking Phase* begins after initialization and runs until the end of *ISAC Phase*. In this phase, active observers measure bistatic range of the mobile target. Then, all these range measurements are sent to corresponding HA, which calculates the location of the mobile target with non-linear least square optimization on triangulation algorithm. A target road-map, which has the target location for each specific time interval, is formed by HA. Using target road-map, HA calculates the target head courses as explained in Section III-B.

Using the target velocity and head course, the HA first creates *image plane*, where a radar image of the mobile target is formed. To form the image, CMTI captures inverse synthetic aperture created by the movement of the target along the multi-static radar structure. Therefore, a matrix, called *Inverse Synthetic Aperture Matrix* ($ISAMatrix$), which consists of all information about anchor-observer pairs whose observations are used in imaging, is formed by HA. This phase is called *Inverse Synthetic Aperture Capturing (ISAC) Phase* and detailed in Section III-C.

According to the $ISAMatrix$, HA asks observer nodes to provide the required observations to the sink. Then, all observations are reliably and energy-efficiently transported to the sink during *Reliable Imaging Observation Transport (RIOT) Phase* as explained in Section III-D.

Once the observation messages are reliably received at sink, the $ISAMatrix$ is regenerated. Based on the information in $ISAMatrix$, a radar image of the mobile target is formed in *Imaging Phase*. In this phase, after all observations are collected, all the related anchor-observer pairs are placed on the image plane. Then, time-domain back-projection based radar imaging algorithm is applied to form a radar image as explained in Section III-E.

A. Initialization Phase

Sink initializes the overall operation of WRSN and starts with localization process. CMTI includes coherent combining of multi-static radar signals. Hence, centimeter (cm)-level localization accuracy is required for high quality imaging. CMTI localization process yields the locations of all anchor nodes through use of Round-Trip Time-of-Arrival (RT-ToA) localization techniques developed for UWB-WSN [17]. To use RT-ToA technique, anchors must be able to retransmit received signal. Then, all observer nodes calculate their distances relative to the anchor nodes using any of the existing TDoA localization techniques[4]. The entire sensor field is divided into clusters by sink using one of the existing energy-efficient, robust and optimum clustering schemes [18] to select *Head Anchors* in the field. However, in CMTI, clustering only means to project the cluster regions for easily selecting HA. After specifying regions, sink determines HA's in their own clusters.

Each anchor sends its location and residual energy to the sink for HA selection. Sink looks for the spatially midmost anchor in the cluster, however, if it has the worst lifetime, sink selects the second midmost one. Then, corresponding HA are specified for each cluster and each one is responsible for the events in its own cluster. Then, sink broadcasts *start detection* message to the nodes in the target detection layer of WRSN. If any event is sensed by the detection nodes, this event record is transmitted to the sink. Then, radar nodes in the location of the event are woken up by sink's *wake up* message. Once the target is detected, target tracking phase of CMTI is invoked and the nearest HA to the event field takes the responsibility of the detection.

Observers take observations from the environment with specific time intervals, i.e., T_σ as described in Section II. These

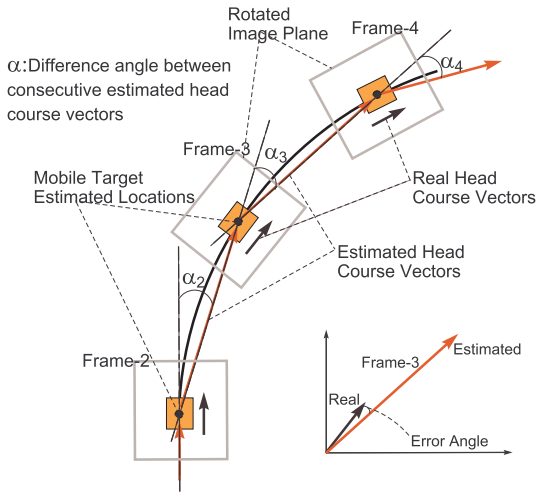

Fig. 2. Head course calculation operation.

observations taken with period of T_σ are called *frame*. Hence, according to the frame frequency, $F_t = 1/T_\sigma$, observers continue to take observations from the environment frame by frame during the entire CMTI operation. Frames are used in tracking process and only few of them are used for imaging process, which are called as *picture*. Therefore, each *picture* used in CMTI can be taken with different frequency as F_p.

B. Target Tracking Phase

Target Tracking Phase is operated concurrently with *ISAC Phase*. After *wake up* message is broadcast by sink, each anchor broadcasts *pilot* message to the observers in its own radar range. *Pilot* message includes the number of the anchor and its location. Observers receiving *pilot* messages calculate their distances to the corresponding anchors.

Tracking is operated in 2D coordinates, hence, only 3 ellipsoid equations suffice to determine the target location. As long as, $N_{anc}\,N_{obs} \geq 3$, where N_{anc}, N_{obs} are the numbers of the awake anchors and observers, respectively, all observers determine the mobile target distance with measurements of TDoA from target. Then, observers send the time and range measurement data to the HA to be used in tracking process. For target localization, HA collects all range measurements from the alerted observers with the frame frequency, F_t.

Using the received range measurements, HA calculates target location (u_x^i, u_y^i) for frame i with non-linear least square optimization on triangulation algorithm through Taylor Series (TS) method. As TS is an iterative method, to avoid divergence, the center of gravity of the alerted radar sensor map is calculated by HA as a good guess for an initial position.

Observers continue to pack the time and range data up with F_t and send to the HA for tracking. Meanwhile, all observers begin to record their observations with time tag, and they keep these records until the sink requests in imaging phase.

After the mobile target locations for each frame is estimated, to determine Head Course Vectors (HCV) indicating the heading of the target for each frame, each location is processed with the proceeding frame location of the target. Estimated HCVs can be drawn as a vector from n^{th} to $(n+1)^{th}$ target location point and real HCVs show the direction of mobility as in Fig. 2. Hence, there should be $(n+1)$ frames to estimate head courses, when total HCV number is n. To avoid blurry radar images, the direction of mobility and target HCV are assumed to be in the same direction for each frame.

HA calculates HCVs for each frame. Based on the difference angle between consecutive estimated HCVs, α, image plane, which is determined to form target radar image, is moved and rotated with respect to direction varying on the consecutive HCVs frame by frame as in Fig. 2.

C. Inverse Synthetic Aperture Capturing (ISAC) Phase

In this phase, a 4×360 matrix, i.e., *Inverse Synthetic Aperture Matrix* ($ISAMatrix$), consisting of anchor and observer numbers with related picture number, is filled with respect to the corresponding bistatic bisector angle by HA of alerted cluster. Bistatic bisector angle, i.e., the angle between a line that bisects the bistatic angle and a reference line, θ, bistatic angle, β, anchor-observer distance, L, are shown in Fig. 3.

Image plane having the target in the middle is virtually moved and rotated by the HA to find θ of each observation, for difference angles, α, frame by frame as in Fig. 2. Recall that each anchor-observer pair yields a bistatic radar structure. However, some of the observed perspectives may degrade the radar image quality. Thus, the best anchor-observer pairs for each perspective must be selected. Here, the anchor-observer pairs, which contribute the most towards maximizing the quality of the radar image, are selected as outlined in Algorithm 1.

Note that radar range resolution (ΔR) mainly dominates the radar image quality. The bistatic range resolution, ΔR_B, of any anchor-observer pair varies with the bistatic angle β, i.e., the angle between anchor-observer pair with the vertex at the target [3] as in Fig. 3. CMTI gets observations with random perspectives. Thus, anchor-observer pairs are placed into the $ISAMatrix$ with respect to their θ to the target.

In *ISAC Phase*, anchor-observer pairs with the smallest bistatic range resolution are selected to be included in the image formation process. For a monostatic radar case, the range resolution is $\Delta R_M = cPW/2$. However, for a bistatic case, for an approximate method [13], this relation becomes,

$$\Delta R_B \approx cPW/\left[2(1+cos(\beta))\right]^{1/2} \tag{8}$$

According to bistatic radar range resolution, with a threshold, CMTI algorithm avoids selection of anchor-observer pairs with large range resolution, and selects appropriate pairs with the smallest range resolution, for each bisector angle to the target. Based on the simulation results, the threshold on range resolution can be selected as cPW. This selection component is called *Smallest Range Resolution Selection with threshold* (SRRS-th) and improves radar image quality.

CMTI captures the inverse synthetic aperture of WRSN as target moves. Based on the SRRS-th component, $ISAMatrix$ is filled with anchor and observer numbers picture by picture. Then, HA decides the size of each observation to be transferred to the sink. In fact, only target radar response part of the observation is essential for imaging. With moving target filter, target radar response can be distinguished to specify target

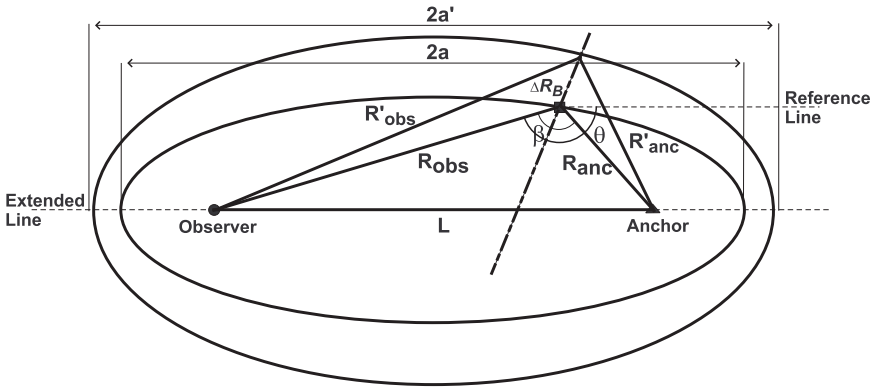

Fig. 3. Bistatic radar structure. β, bistatic angle and θ, bisector angle.

Algorithm 1: ISAC SRRS-th algorithm. α and γ are the angles between the anchors and observers LoS to target and reference line. $noanc$, $noobs$, and $nopic$ are total number of anchor, observer, picture, respectively.

$ISAMatrix = zeros(4, 360)$
$BiRes = zeros(nopic, noanc, noobs)$ /*bistatic range resolution */
for $h = 1 : nopic$ **do**
  for $g = 1 : noanc$ **do**
    α=CalcLOS(g^{th}, h^{th})
    for $w = 1 : noobs$ **do**
      γ=CalcLOS(w^{th}, h^{th})
      $\theta = (\alpha + \gamma)/2$ /*Find bisector/bistatic angles (θ,β)*/
      $\beta = (\alpha - \gamma)$
      $BiRes(h, g, w) = (c \times PW)/(sqrt(2(1 + cos(\beta))))$
      if $BiRes(h, g, w) > (c \times PW)$ **then**
        go to next iteration /*Not use anchor-observer pair*/
      end
      if $ISAMatrix(1, \theta) == 1$ **then**
        $[w_{ex}; h_{ex}; g_{ex}] = ISAMatrix(2 : 4, \theta)$
        /*Select the Smallest Range Resolution*/
        if $BiRes(h, g, w) < BiRes(h_{ex}, g_{ex}, w_{ex})$ **then**
          $ISAMatrix(2 : 4, \theta) = [w; h; g]$
        end
        go to next iteration
      end
      $ISAMatrix(1 : 4, \theta) = [1; w; h; g]$
    end
  end
end

features. As explained in Section III-B, observers measure the target distance. Based on these measurements, CMTI adopts time-domain window at observer, i.e., *target observation window*, W, on the target radar response of each observation to decrease communication overhead.

To specify length of W, firstly, HA checks the range measurements used in *target tracking phase* and searches the ones taken by the observers already in $ISAMatrix$. If any of the range measurements cannot be found, HA requests the missing one from the corresponding observer. Using range measurements, HA calculates the longest target range profile, based on which it determines and broadcasts length of W to all alerted observers.

According to the anchor, observer and picture numbers in the $ISAMatrix$ and W length, HA informs the alerted observers by sending the number of the observations which should be sent to the sink.

D. Reliable Imaging Observation Transport (RIOT) Phase

The objective of this phase is to assure that observers reliably send their observations to sink, which constructs a high quality target radar image with minimum energy cost. Three types of packets, i.e., observation transport (OTP), range measurement (RMP), and CMTI control packets (CCP) are used. OTP carry the imaging observations to the sink, with perspective number, anchor and observer number, picture number and the packet location (PL:2bytes) in entire observation. If observation size (l_{OBS}) is larger than the packet size, entire observation is divided into small blocks with length k and 7 bytes header. OTP header also contains bistatic bisector angle in which the target is observed (BN:2bytes). Anchor (AN:1byte), observer (ON:1byte) and picture (PN:1byte) number fields are used for sending $ISAMatrix$ information.

RMP carry target distance, anchor and observer number, 6 bytes header as well as the information of corresponding anchor-observer pair. RMP header contains AN, ON, Range measurement Time (RT:3byte) and Range measurement Number (RN:1byte). The rate of these packets is specified by control packets sent by the HA in the tracking phase. RMP is sent from observers to HA, which is generally at one hop distance. CCP provide the control of the entire operation and inform observers of transition between CMTI phases.

Each observation is independent and has the same importance for radar imaging. Further, traffic generated by observers is not very high. Thus, none of the existing solutions for reliability in WSN [22] is applicable for CMTI. Moreover, evaluation of retransmission and forward error correction (FEC)-based mechanisms in WSN reveal that for low bit-error rate channel, erasure coding is both energy-efficient and more reliable, however, it compromises energy-efficiency for reliability under high packet error rates (PER) [19], [20]. Hence, for RIOT phase, retransmission-based automatic repeat request (ARQ) and FEC approaches are compared in terms of energy-efficiency [21]. Based on the energy-efficiency metric defined in [21], a suitable metric that captures the energy and reliability constraints is adopted for CMTI such that $\eta_{CMTI} = [E_{eff}/E_{total}]r_{obs}$, where E_{eff}/E_{total} is the energy throughput, $r_{obs} = (1 - OER)$ is the observation acceptance rate and OER is the observation error rate. Fig. 4 shows η_{CMTI} for ARQ and different Reed-Solomon (RS) codes. For typical neighbor distances of 20$\sim$30 meters in

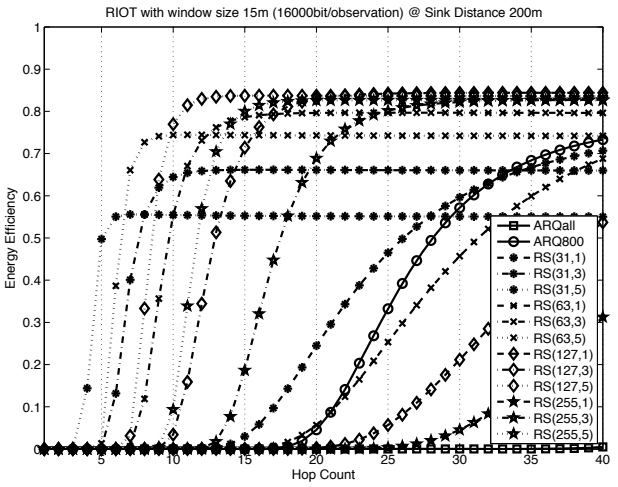

Fig. 4. Energy efficiency vs. hop count with ARQ & FEC with RS codes.

WSN [21], typical hop count varies from 7 to 10 hops when node to sink distance is $200m$. Clearly, at these hop counts, RS(63,5) code is more energy-efficient for CMTI. Thus, results reveal that FEC, e.g., with RS(63,53,5), could be used to achieve high energy-efficiency and reliable delivery of observations for maximum window size, $W = 15m$.

Sink receives OTP messages from observers, and then, according to anchor-observer pair and perspective numbers in each OTP, it regenerates the $ISAMatrix$. Despite packet losses, observations can be reconstructed to a certain extent with the help of FEC scheme. A small decrease on the number of observations slightly degrades radar image quality, which is unlikely to affect the target classification performance.

E. Imaging Phase

2D image of the target is required to specify the target's shape and features. 1D profile of the target can be easily extracted from time-domain calculation of received signal using only range-profile of the target. The second dimension involves more calculation in frequency-domain using Doppler-profile of the target [2]. However, obtained range profiles with different target perspectives can be used to form 2D image. Instead of frequency-domain calculations, radar images are created by CMTI based on *kirchhoff migration* techniques such as *standard back-projection* (*SBP*), *cross-correlated back-projection* (*CBP*) [10] and its modified version [11], which are suitable for multi-static radar imaging [4].

SBP approach uses coherent sum of sampled radar returns of array elements [10]. It projects the spatial coordinates of transmitter and receiver antenna to the image plane, and then, correlates transmitter, receiver and the pixel to the range profiles of receivers. This yields acceptable results in short-range applications, however, produces smeared images for larger distances [10]. CBP algorithm yields a better cross-range by correlating the range profiles. It generates a signal for the specific pixel location by coherent sum of cross-correlation between the main and reference channels. Resulting signal eliminates the smearing at the SBP image [10].

Once the displayed area size on image plane is set, perspectives are selected by checking the first row of $ISAMatrix$. Image plane width and length are specified in pixels. For each pixel location (i, j), the time of flight (ToF) of pulses are calculated for each perspective. Amplitude of the received signal from the anchor of the observer at the corresponding ToF for the picture is recorded. As a reference channel is required to correlate channels, a reference observer is chosen among alerted observers, of which pulses are transmitted from the same anchor at the same picture. However, selection is made on the verticalness of the perspective to anchor-observer pair. Moreover, for using the modified version of CBP, CMTI finds additional reference observer. Then, recorded observation signals from three channels are cross-correlated for the pixel (i, j). These values are saved, and added for each perspective. After all perspectives are processed for pixel (i, j), the sum is assigned to the value of the pixel (i, j). This process is repeated for each pixel to form the target radar image.

IV. Error Analysis

Here, we analyze the sources of error that may affect the radar image quality. Noise is the main limitation of radar measurements. Receivers must have large SNR for accurate measurements. $R_B = (R_{anc} + R_{obs})$, the distance of anchor-target-observer multi-path, is the measurement of time delay for the anchor's radar signal, traveling from the target to observer. With error-free propagation speed of light c, range error is, $\delta R_B = c\,\delta T$, where δT is the delay error.

Range measurement is based on locating the leading edge of the pulse [1], which can be corrupted by the noise, and hence, slightly drifted. This drift depends on the receiver side SNR. Hence, range measurement error can be calculated with respect to SNR. Using (3), SNR in bistatic radar structure is expressed as [5],

$$SNR_{Bistatic} = (P_{anc}\,C)\,/(R_{anc}\,R_{obs})^2 \tag{9}$$

where C is a radar constant, i.e.,

$$C = \frac{N_s\,G_{anc}\,G_{obs}\,\sigma_B\,c^2}{N_0\,PRF\,(4\pi)^3}\left(\frac{1}{f_L} - \frac{1}{f_L + B}\right) \tag{10}$$

As PRF and antenna gains of both nodes are constant, C is constant. Thus, SNR depends only on P_{anc} and $(R_{anc}\,R_{obs})$.

Time-delay error is the root mean square (rms) error between the measured and actual values stated as [1],

$$\delta T = 1/\left[\chi\sqrt{2SNR}\right] \tag{11}$$

where χ is effective bandwidth of received waveform [1], i.e.,

$$\chi^2 = \frac{\int_{-\infty}^{\infty}(2\pi f)^2\,|S(f)|^2\,\mathrm{d}f}{\int_{-\infty}^{\infty}|S(f)|^2\,\mathrm{d}f} \tag{12}$$

Normal Gaussian pulses are transmitted by the anchor, and the second derivative of the transmitted pulses are received, due to the effect of channel and observer antenna. A typical value for the compressed Gaussian pulses effective bandwidth is used as $5.2/PW$, where PW is the pulse-width.

SNR is not constant for all points on equi-ToA ellipse. With bistatic angle β, SNR and thus, range measurement error may vary. For the maximum error, it is calculated as β is maximum.

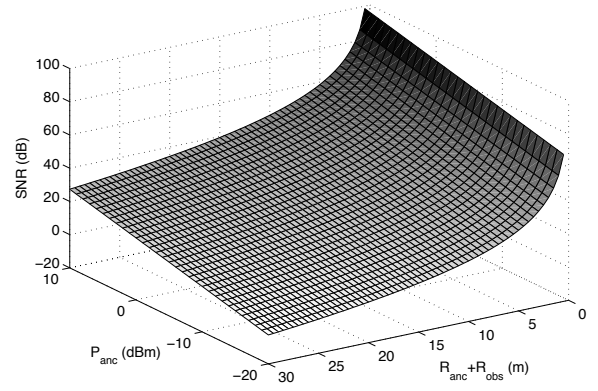

(a)

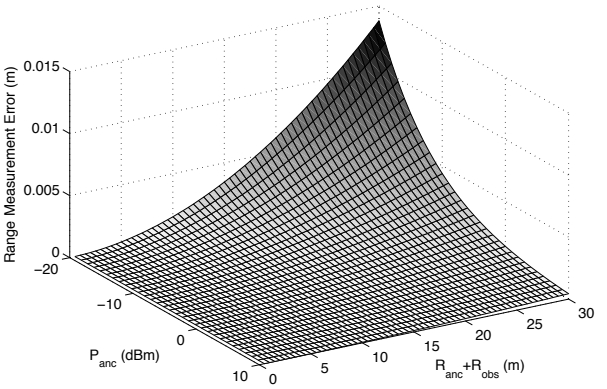

(b)

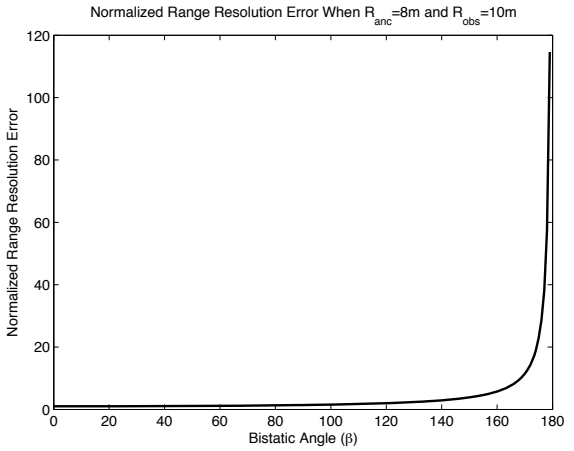

(c)

Fig. 5. Bistatic (a) SNR, (b) range measurement error vs. P^{anc} and $(R_{anc}+R_{obs})$, (c) normalized range resolution error vs. β.

Hence, R_{anc} is equal to R_{obs}, and then, $(R_{anc}\, R_{obs})$ can be expressed as $(R_B)^2/4$. The rms range measurement error is $c \times \delta T$ and by substituting (9) into (11),

$$\delta(R_{anc}+R_{obs}) = c\,(R_B)^2 \,/\, \left[4\,\chi\,\sqrt{2\,P_{anc}\,C}\right] \qquad (13)$$

To observe the range measurement error incurred during the ranging process, we use typical UWB radar sensor parameters in Table I in (13). The range measurement error for P_{anc} and $(R_{anc}+R_{obs})$ are shown on Fig. 5(b). Hence, if P_{anc} is around $-20dBm$, then ranging error becomes nearly $1.4cm$ at maximum range $30m$. For the values in Table I, P_{min}^{anc}, as explained in Section II, can be found as $0.184mW$, $-7.35dBm$. Thus, when P_{min}^{anc} is transmitted at anchor, only $3mm$ ranging error is observed at $30m$ maximum bistatic range.

TABLE I
UWB RADAR SENSOR & CHANNEL PARAMETERS

RG_w	observer range-gate width	$50ps$
PW	anchor pulse-width	$0.5ns$
R_{max}	maximum bistatic range	$30m$
B	Bandwidth	$2GHz$
f_L/f_U	lower / upper frequency	$1.5/3.5GHz$
N_s	processing gain	$10dB$
G_{anc}/G_{obs}	anchor / observer antenna gain	$0dB$
SNR_{th}	threshold SNR	$10dB$
S_{max}	maximum number of samples	2000
V_{max}	maximum sensible velocity	$28m/s$
F_{ADC}	A/D converter sampling rate	$1.5MHz$
T_σ	time for complete signal	$1.33ms$
T_s	observer receiver temperature	$290K$
NF	observer receiver noise figure	$7dB$
N_0	noise power at the observer	2×10^{-20}
PRF	anchor pulse repetition frequency	$1.5MHz$
P_{min}^{anc}	minimum anchor transmitted power	$-7.35dB$

Another source of error is *range resolution error*. This is the difference between monostatic and bistatic radar resolutions, which directly affects radar image quality. This normalized error can be expressed as, $\epsilon = (\Delta R_B - \Delta R_M)\,/\,(\Delta R_M)$, where ΔR_M and ΔR_B are the monostatic and bistatic range resolutions, respectively. As in Fig. 5(c), as β approaches 180 degrees, range resolution error significantly increases. To mitigate this, CMTI adopts the smallest range resolution selection with threshold (SRRS-th) algorithm, which mainly selects anchor-observer pairs with smaller bistatic angle β.

V. PERFORMANCE EVALUATION

Simulations are done in MATLAB. Radar sensor nodes are uniformly distributed to known locations over a $150m \times 150m$ WRSN topology with the anchor to observer ratio of 25%. Sensor field is mapped to a 2000×2000pixels. Mobile target is modeled as a basic point scatterer [14], and composed of multiple point targets with constant $1m^2$ RCS. To simulate time-invariant clutter effect, 250 1-point spatially static clutters with $0.5m^2$ RCS are randomly deployed over the field.

An UWB radar is simulated, as a 0.5 nanosecond compressed Gaussian impulses are generated by anchors with power P_{anc}^{min} and received by each observer impulse receiver with free space conditions. Radar sensor parameters are used as in the Table I. Performance evaluations of CMTI are done with its smallest range resolution selection with threshold (SRRS-th), without threshold (SRRS), and no selection on range resolution (NoSEL) components.

For simulations with varying average sensor density, a 1-point target moves with the $2m/s$ velocity for $10s$ over the field deployed with $8-20$ sensors, when picture frequency, F_p, is $1Hz$. For experiments with varying target velocity, the same target moves with the velocities $1-28m/s$ for $10s$ over the field with 12 sensors. RS(63,5) FEC scheme is adopted in the RIOT phase, when end-node to sink distance is $200m$ and

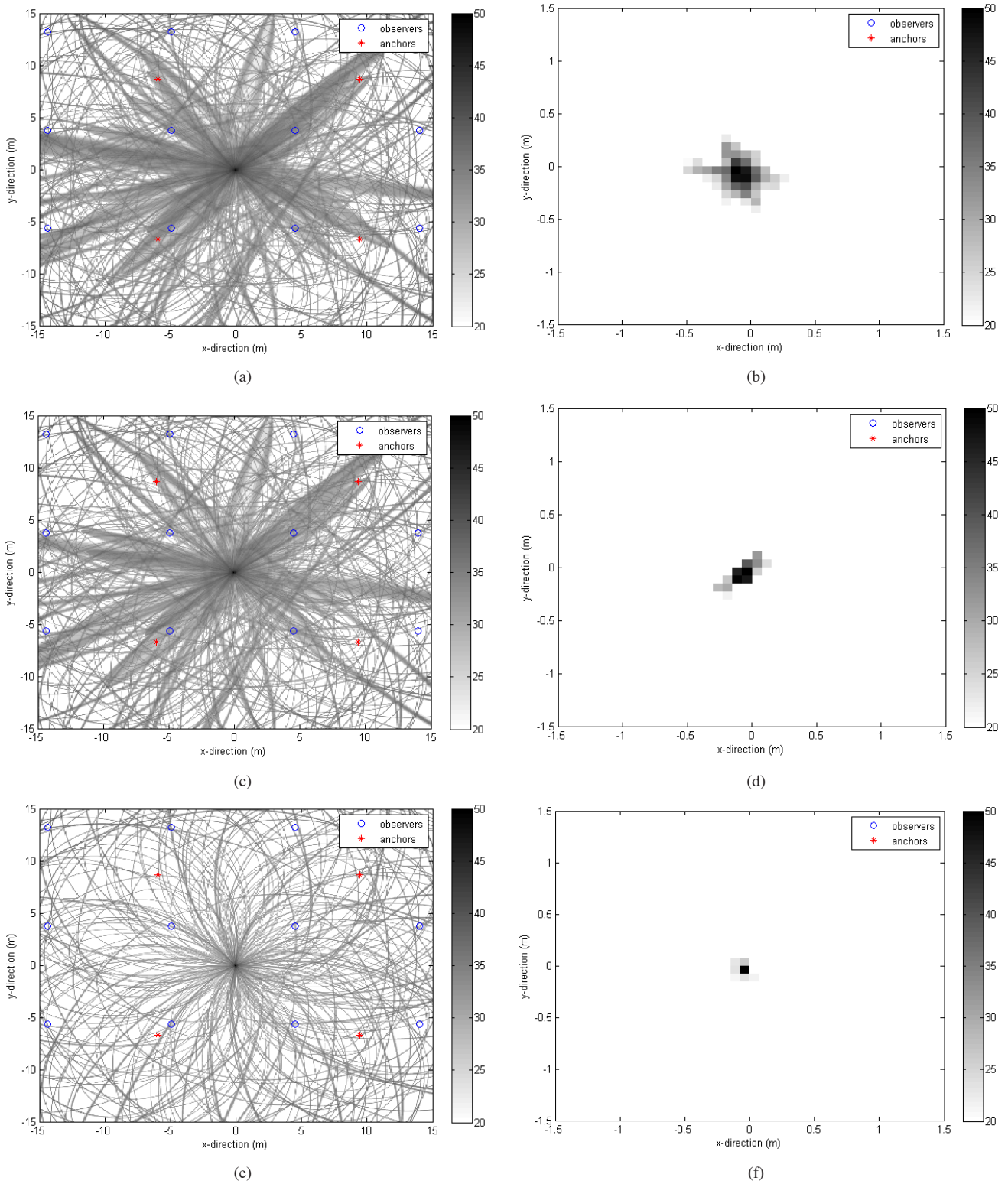

Fig. 6. 1-Point mobile target radar image with SBP/CBPbased CMTI with NoSEL (a,b), SRRS (c,d), SRRS-th (e,f). (b,d,f) are the windowed radar images.

hop count to sink is 10. Corresponding bit error rate (BER) is approximately 7×10^{-4} for NCFSK modulated data under flat fading, for typical neighbor distances $20m$ in WSN as stated in [21]. All radar nodes are assumed to be static. Each data point on the plots represents 10 run of the simulation. A line fitting of data points is overlaid on each plot.

A. Imaging Performance

CMTI performance is evaluated for different target point scatterer models. For 1-point target on a linear road with the velocity $2m/s$, 10 pictures are used in imaging during 6 seconds and mobile target is tracked with only average $2cm$ error. 13 anchors and 29 observers are alerted in the field.

Non-windowed results of CMTI with selection components

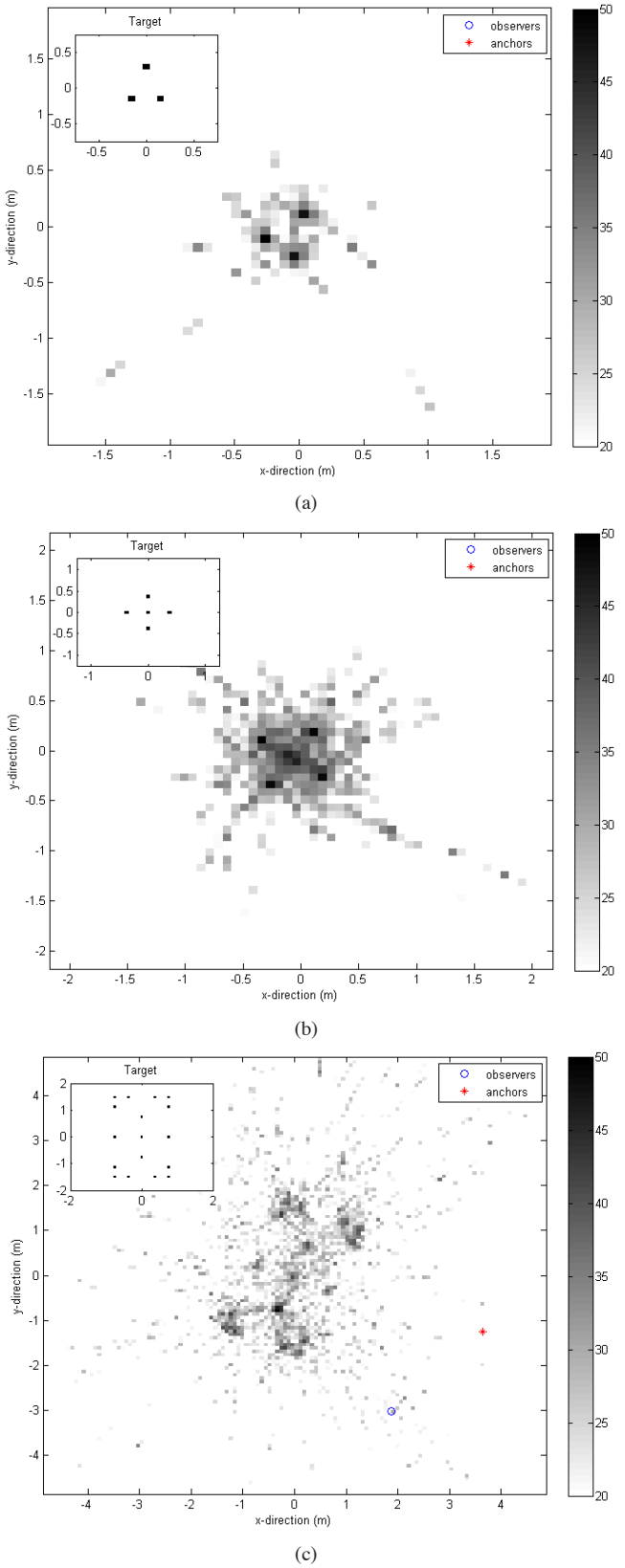

Fig. 7. 3-Point (a), 5-Point (b) & 17-Point (c) mobile target radar images with modified CBP-based CMTI with SRRS-th.

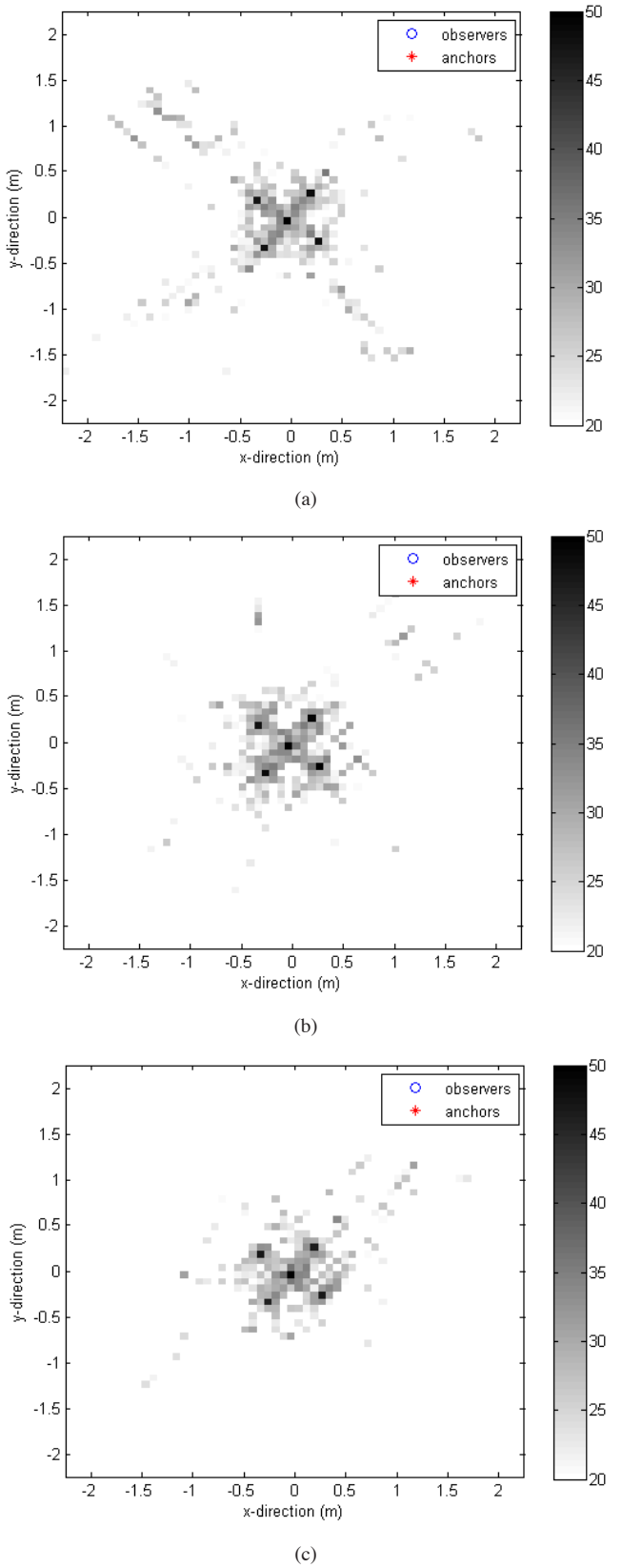

Fig. 8. 5-Point target radar images with mobile target velocity $2.5m/s$ (a), $7.5m/s$ (b) and $15m/s$ (c).

NoSEL, SRRS and SRRS-th, in Fig. 6(a), 6(c), 6(e), are 400×400 pixels radar images spanning $30m \times 30m$ field. Due to SBP, these images have very high side-lobe values around the point. In Fig. 6, observers and anchors locations relative to target at first picture are indicated. In Fig. 6(a) and 6(c), obviously the side-lobe values are very high, thus,

target can be hardly recognized. On the other hand, resulting windowed images for NoSEL, SRRS, SRRS-th with imaging algorithm based on modified CBP are shown in Fig. 6(b), 6(d), 6(f). NoSEL totally ruins the radar image, because many anchor-observer pairs have very high bistatic range resolutions. Besides, SRRS radar image has higher quality than NoSEL, however, only few anchor-observer pairs degrade the image. SRRS-th radar image has the highest quality and the target can be clearly seen in the windowed radar image on Fig. 6(f).

CMTI performance is also shown for 3, 5, 17-points targets in Fig. 7. Radar image size increases with target dimensions as CMTI increases target window size from small target to larger target. For the 3, 5-points targets, each point can be clearly distinguished as in Fig. 7(a) and 7(b). Shape and dimensions of 17-points target can be extracted from the image in Fig. 7(c). Simulations are also run to show the performance with 5-point target for varying velocity. As in Fig. 8, radar images do not experience quality loss due to target velocity, and can be used to specify mobile target features.

B. Average Range Resolution

We measure the *normalized range resolution error* of bistatic radar structure with respect to the monostatic radar range resolution ΔR_M, which is expressed as,

$$\epsilon_t = \sum_{n=1}^{Nobs} \frac{(\Delta R_B - \Delta R_M)/(\Delta R_M)}{Nobs} \tag{14}$$

where $Nobs$ is the number of observations taken by CMTI.

As in Fig. 9(a), SRRS-th has the minimum range resolution and almost the same as monostatic range resolution. SRRS-th performance decreases with increasing sensor density. SRRS reaches to SRRS-th performance for dense network deployment. NoSEL performs nearly 2.5 times worse than monostatic range resolution. For varying target velocity, as in Fig. 9(c), range resolution is not affected, and SRRS-th maintains its quality despite an increase in target velocity.

C. Tracking Mean Square Error

The error between estimated and actual target locations, i.e., *tracking mean square error* is expressed as

$$\sigma_t^2 = \sum_{i=1}^{N} \frac{(\hat{x}_i - x_i)^2 + (\hat{y}_i - y_i)^2}{N} \tag{15}$$

where N is the number of frames, (x_i,y_i) and $(\hat{x}_i,\hat{y}_i)$ are actual and estimated target locations at frame i, respectively.

As the target is placed on image plane based on tracking result, radar image gets blurred if the tracking error is high. The performance depends on the total number of range measurements used in target tracking phase. As in Fig. 9(b), increase in sensor density reduces tracking error as it increases the total number of range measurements to be used in tracking process. Nevertheless, for varying target velocity, as in Fig. 9(d), tracking error remains almost constant as *target tracking phase* is completely independent of *ISAC Phase* in CMTI.

D. Communication Overhead

Communication overhead is defined as the total data sent by alerted observers to the sink for imaging process, i.e.,

$$D_{total} = l_{OBS}\, Nobs \tag{16}$$

where l_{OBS} is the data length of the observation and $Nobs$ is the number of the observations to be taken.

As observed in (16) and shown in Fig. 9(e), overhead increases with the number of the observations and sensor density. However, as explained in Section III-C, $ISAMatrix$ perspective size is limited to 360, therefore, only 360 perspectives can be used for imaging, which bounds the total communication overhead for lower sensor densities.

As seen in Fig. 9(f), communication overhead increases until the maximum number of observations is reached at higher velocities from $5m/s$ to $28m/s$. Thus, CMTI is not affected by excessive target velocity and network density. Furthermore, (16) shows that overhead also depends on data length of the observation, which only changes with observation window size depending on dimensions of the target.

E. Energy Consumption

Energy consumption by communication in CMTI can be mainly divided into two parts, i.e., due to communication of observation transport (OTP) and range measurement packets (RMP). Here, RMP and OTP are sent with FEC scheme RS(63,5). CMTI control packets (CMP) energy consumption is assumed to be negligible. Energy consumption of the OTPs,

$$E_{OTP} = E_{OTP}^{obs}\, Nobs \tag{17}$$

where E_{OTP}^{obs} is the amount of energy consumed in sending one observation and $Nobs$ is the number of the observations to be taken in the field by alerted observers. For the RMPs,

$$E_{RMP} = E_{RMP}^{r}\, N_{anc}\, N_{obs}\, F_t\, T_{total} \tag{18}$$

where E_{RMP}^{r} is the energy of sending one range measurement, N_{anc} and N_{obs} are the average number of the alerted anchors and observers, respectively, F_t is the frame frequency and $T_{total} = 10s$ is the total time for $ISAMatrix$ capturing. Then, total energy consumption is given by

$$E_{CMTI} = E_{OTP} + E_{RMP} \tag{19}$$

Accordingly, we observe (19) for varying sensor density and target velocity. Here, $T_{total} = 10s$ and $F_t = 100Hz$ are kept constant. As observed from (17), (18), and (19), total energy consumption mainly depends on the number of observations and the total number of alerted observers. Besides, E_{OTP} mainly dominates the energy consumption as amount of observation data is higher than range measurement data. As seen in Fig. 9(g), total energy consumption increases with the sensor density. For varying mobile target velocity, as seen in Fig. 9(h), energy consumption performance is observed to be similar to communication overhead metric as expected.

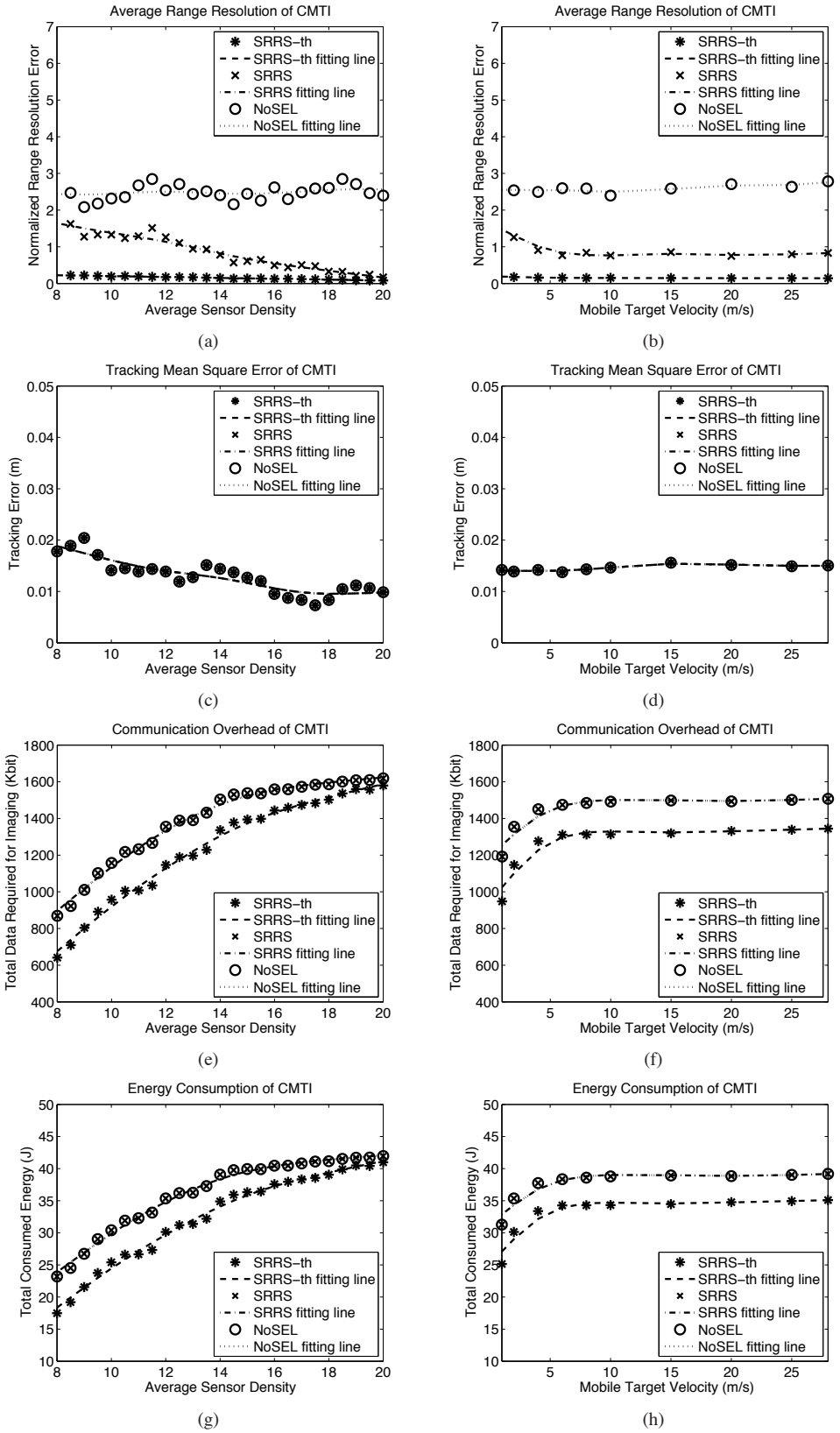

Fig. 9. (a,b) range resolution error ϵ_t, (c,d) tracking error σ_t, (e,f) data used for imaging D_{total}, (g,h) total energy E_{CMTI} vs. sensor density, target velocity.

VI. Conclusions

In mission critical surveillance systems, among various target classification methods, imaging of target yields the most valuable information to specify the threat level of the intrusion. In this paper, an architecture and a new collaborative mobile target imaging (CMTI) algorithm for WRSN are presented.

CMTI algorithm can accurately and efficiently obtain an image of mobile targets based on the collaborative effort of deployed UWB wireless radar sensor nodes. Performance evaluations reveal that CMTI algorithm yields high quality radar image of mobile targets in WRSN with very low communication overhead, using observation windowing, reliability and energy expenditure, using FEC. Experiment results show that its performance is not affected by the shape and velocity of mobile targets and the channel conditions.

REFERENCES

[1] M. I. Skolnik, "Introduction to Radar Systems," *McGraw-Hill Higher Education*, Third Edition, 2001.

[2] D.R. Wehner, "High Resolution Radar," *Artech House,* 1987.

[3] N.J. Willis, "Bistatic Radar," *Scitech Publishing Inc.*, 2005.

[4] R.S. Thoma, O. Hirsch, J. Sachs, R. Zetik, "UWB Sensor Networks for Position Location and Imaging of objects and Environments," in *Proc. EUCAP'07*, November 2007.

[5] E. Paolini, A. Giorgetti, M. Chiani, R. Minutolo, M. Montanari, "Localization Capability of Cooperative Anti-Intruder Radar Systems," in *Proc. EURASIP'08*, March 2008.

[6] P.K. Dutta, A.K. Arora, and S.B. Bibyk, "Towards Radar-Enabled Sensor Networks," in *Proc. IPSN'06*, April 2006.

[7] S. Azevedo, T.E. McEwan, "Micropower Impulse Radar," in *Science & Technology Review*, January/February, 2006.

[8] J. Sachs, M. Kmec, R. Herrmann, P. Peyerl, P. Rauschenbach, "An Ultra-Wideband Pseudo-Noise Radar Family integrated in SiGe:C," in *Proc. IRS'06*, May 2006.

[9] J. Sachs, P. Peyerl, R. Zetik, S. Crabbe, "M-Sequence Ultra-Wideband-Radar: State of Development and Applications," in *Proc. IEEE Radar 2003*, Australia, September 2003.

[10] S. Foo, S. Kashyap, "Cross-correlated back projection for UWB radar imaging," in *Proc. AP-S 2004*, Volume 2, pp. 1275-1278, June 2004.

[11] R. Zetik, J. Sachs, R. Thoma, "Modified Cross-Correlation Back Projection for UWB Imaging: Numerical Examples," in *Proc. ICU 2005*, September 2005.

[12] C. Chang, A. Sahai, "Object Tracking in a 2D UWB Sensor Network," in *Proc. ACSSC'04*, vol. 1, pp. 1252-1256, USA, November 2004.

[13] M. Tobias, A.D. Lanterman "Probability Hypothesis Density-Based Multitarget Tracking With Bistatic Range and Doppler Observations," in *Proc. IET RSN 2005*, vol. 152, issue 3, pp. 195-205, June 2005.

[14] N.J. Mohamed, "Target Signature Using Nonsinusoidal Radar Signals," *IEEE Trans. EMC*, vol. 35, no. 11, pp. 457-465, November 1993.

[15] R. Zetik, S. Crabbe, J. Krajnak, P. Peyerl, J. Sachs, R. Thoma, "Detection and Localization of Persons Behind Obstacles Using M-sequence Through-the-wall Radar," in *SPIE, Sensors, and C3I Technologies for Homeland Security and Homeland Defense*, vol. 6201, May 2006.

[16] H. Sheng, P. Orlik, A.M. Haimovich, L.J. Cimini, and J. Zhang, "On the Spectral and Power Requirements for Ultrawideband Transmission," in *Proc. ICC'03*, vol. 1, pp. 738-742, USA, May 2003.

[17] G. Mao, B. Fidan, B. Anderson, "Wireless Sensor Network Localization Techniques," in *Computer Networks Journal (Elsevier)*, vol. 51, no. 10, pp. 2529-2553, July 2007.

[18] D. Wei, H.A. Chan, "A Survey on Cluster Schemes in Ad Hoc Wireless Networks," in *Proc. IEE Mobility Conference*, GuangZhou, 2005.

[19] S. Kim, R. Fonseca, D. Culler, "Reliable Transfer on Wireless Sensor Networks," in *Proc. IEEE SECON 2004*, pp. 449-459, October 2004.

[20] H. Wen, C. Lin, F. Ren, Y. Yue, X. Huang, "Retransmission or Redundancy: Transmission Reliability in Wireless Sensor Networks," ,n *Proc. IEEE MASS 2007*, October 2007, pp. 1-7.

[21] Y. Sankarasubramaniam, I.F. Akyildiz, S.W. McLaughlin, "Energy Efficiency Based Packet Size Optimization in Wireless Sensor Networks," in *Proc. IEEE SNPA'03*, 2003, pp. 1-8.

[22] C. Wang, M. Daneshmand, B. Li, K. Sohraby, "A Survey of Transport Protocols for Wireless Sensor Networks," *IEEE Network*, vol. 20, no. 3, pp. 34-40, 2006.

Muharrem Arık (S'10) received his B.S. degree in Electrical and Electronics Engineering from Hacettepe University Ankara, Turkey, in 2005 and M.S. degree in Electrical and Electronics Engineering from Middle East Technical University, Ankara, Turkey, in 2008. He is currently a Electronics Engineer in Radar, Electronic Warfare and Intelligence Division in ASELSAN Inc. and pursuing his Ph.D. degree at the Electrical and Electronics Engineering Department, Middle East Technical University, Ankara, Turkey. His current research interests include radar sensor networks and cognitive radio sensor networks. He received the Thesis of the Year Award 2010 given by Middle East Technical University Graduate School of Natural and Applied Sciences.

Ozgur B. Akan (M'00-SM'07) received the B.S. and M.S. degrees in electrical and electronics engineering from Bilkent University and Middle East Technical University, Ankara, Turkey, in 1999 and 2001, respectively. He received the Ph.D. degree in electrical and computer engineering from the Broadband and Wireless Networking Laboratory, School of Electrical and Computer Engineering, Georgia Institute of Technology, Atlanta, in 2004. He is currently Associate Professor with the Department of Electricaland Electronics Engineering, Middle East Technical University and the Director of Next-generation Wireless Communications Laboratory (NWCL). His current research interests are in wireless communications, bio-inspired communications, nano-scale and molecular communications, network information theory. Dr. Akan is an Associate Editor for IEEE Transactions on Vehicular Technology, Editor for ACM/Springer Wireless Networks (WINET) Journal, International Journal of Communication Systems (Wiley), Nano Communication Networks Journal (Elsevier). He served as an Area Editor for AD HOC Networks Journal (Elsevier) (between 2004-2008), as a Guest Editor for several special issues, as the General Co-Chair for The Third International Conference on Bio-Inspired Models of Network, Information, and Computing Systems (ICST/IEEE BIONETICS 2008), the European Vice Chair for The Second International Conference on Nano-Networks (ICST/ACM Nano-Net 2007), an International Vice Chair for IEEE INFOCOM 2006, and in organizing committees and technical program committees of many other international conferences. He is the Vice President for IEEE Communications Society - Turkey Section. He is an IEEE Senior Member (Communications Society), and a member of ACM. Dr. Akan received the IBM Faculty Award 2008, Turkish Academy of Sciences Distinguished Young Scientist Award 2008 (TUBA-GEBIP).